Bulletin of Electrical Engineering and Informatics
Vol. 13, No. 2, April 2024, pp. 996~1006
ISSN: 2302-9285, DOI: 10.11591/eei.v13i2.5847

A novel women's ovulation prediction through salivary ferning using the box counting and deep learning

Heri Pratikno[1,2], Mohd Zamri Ibrahim[1], Jusak Jusak[2,3]
[1]Faculty of Electrical and Electronics Engineering Technology, University Malaysia Pahang Al-Sultan Abdullah, Pahang, Malaysia
[2]Department of Computer Engineering, Faculty of Informatics Technology, University Dinamika, Surabaya, Indonesia
[3]School of Science and Technology, James Cook University, Singapore, Singapore

Article Info

Article history:

Received Jan 24, 2023
Revised Jul 12, 2023
Accepted Sep 11, 2023

Keywords:

Box counting
Computer vision
Deep learning
Fractal dimension
Pixel counting
Salivary ferning

ABSTRACT

There are several methods to predict a woman's ovulation time, including using a calendar system, basal body temperature, ovulation prediction kit, and OvuScope. This is the first study to predict the time of ovulation in women by calculating the results of detecting the fractal shape of the full ferning (FF) line pattern in salivary using pixel counting, box counting, and deep learning for computer vision methods. The peak of a woman's ovulation every month in her menstrual cycle occurs when the number of ferning lines is the most numerous or dense, and this condition is called FF. In this study, the computational results based on the visualization of the fractal shape of the salivary ferning line pattern from the pixel-counting method have an accuracy of 80%, while the fractal dimensions achieved by the box-counting are 1.474. On the other hand, using the deep learning image classification, we obtain the highest accuracy of 100% with a precision value of 1.00, recall of 1.00, and F1-score 1.00 on the pre-trained network model ResNet-18. Furthermore, visualization of the ResNet-34 model results in the highest number of patches, i.e., 586 patches (equal to 36,352 pixels), by applying fern-like lines pattern detection with windows size 8x8 pixels.

Corresponding Author:

Mohd Zamri Ibrahim
Faculty of Electrical and Electronics Engineering Technology
University Malaysia Pahang Al-Sultan Abdullah
Pahang, Malaysia
Email: zamri@umpsa.edu.my

1. INTRODUCTION

The main contribution to this research is to apply and develop methods to predict women's ovulation time by computing images of salivary ferning objects using box counting, pixel counting, and deep learning for computer vision. The first problem in this study is detecting fern-like lines in saliva with a transparent layer, irregular shapes, and lighting on the surface, as shown in Figure 1(a). In previous studies, the salivary ferning image segmentation process was carried out using the frangi filter [1], shown in Figure 1(b). The second problem in this study is how to predict a woman's ovulation time through full ferning (FF) images on salivary ferning images every month during a woman's menstrual cycle. One of the main challenges in predicting the time of ovulation in this study is the level of hormonal fertility, which is different from the calendar menstrual cycles of women each month. Several factors affect the hormones progesterone and estrogen, including stress levels, smoking, fatigue, and alcoholic beverages. Conventional methods commonly used to detect ovulation time include calculating the menstrual cycle calendar system, ovulation predictor kits, test packs, basal body temperature, OvuScope, and analysis of cervical fluid.

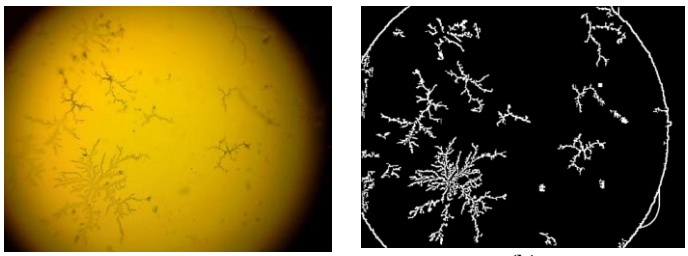

(a) (b)

Figure 1. Fern-like lines display for; (a) salivary ferning and (b) frangi filter segmentation results

Another research is linear with determining the time of ovulation through salivary ferning using an infrared thermometer sensor connected to a microcontroller through temperature and time parameters; the weakness of this tool is that it is still in prototype form, and it is difficult for ordinary people to operate it [2]. Predicting a woman's ovulation period through saliva images using a conventional image processing method approach using the J48 decision tree algorithm in the weka program [3]. Ovulation detection research related to salivary crystallization patterns to detect estrus in eight female bubalus bubalis buffaloes for three months [4]. Research studying the menstrual cycle of three female bornean orangutans related to the relationship between fertility and salivary crystallization [5]. Another study predicts female ovulation through artificial saliva and human saliva through smartphone-based hardware and microfluidic devices [6], a survey that detects and predicts ovulation by measuring the temperature in the ear canal using an in-ear thermometer every 5 minutes during sleeping hours, then the results are sent to the smartphone for analysis [7].

Fractal analysis has become a popular method in all branches of scientific inquiry, including biology and medicine. Discuss some basic principles related to fractal analysis and building meaningful relationships between fractal analysis and geometry [8]. Fractal analysis is a mathematically independent and experimental method based on the mandelbrot fractal geometry, traditional euclidean experimental geometry, and the richardson coastline method. Morphometrics is an integral part of most modern morphological studies, which are widely used in research in the field of medicine [9]. In the last decade, the principles, parameters, and methods of fractal geometry have been increasingly used in morphological studies rather than euclidean geometry. The fundamental parameter of fractal geometry is the fractal dimension. Fractal dimensions allow it to measure the degree of space filling with particular geometric objects and characterize the complexity of its spatial configuration. Many anatomical structures with complex irregular shapes cannot be described clearly and comprehensively by traditional geometric and morphometric methods and techniques: rare linear forms, uneven surfaces of various structures, structures with complex branching, tree-like structures, reticulated, porous structures, and others.

The fractal dimension is a valuable and informative morphometric parameter that can complement existing quantitative parameters for measuring objective characteristics of various anatomical structures and pathological foci. Qualitative fractal analysis can complement existing morphometric methods and techniques and allow a comprehensive assessment of the degree of complexity of the spatial configuration of disordered anatomical structures. Devi and Vidivelli [10] proposes a modified differential box counting (MDBC) method to process breast cancer images using box overcounting and undercounting, which cover all images with the required scale. In the MDBC way, selecting the appropriate box size and calculating the under counting shifting rule address the problem of overcounting.

In this study, in addition to calculating the fractal dimensions of salivary ferning using pixel counting and box counting, the process of calculating fern-like lines detection in salivary ferning using computer vision or patch windows is also carried out in computing in deep learning. Based on previous research [11] that compared fifteen pre-trained convolutional neural network (CNN) models to detect and visualize the shape of fern-like lines patterns from salivary ferning images with a size of 578x814 pixels, ResNet50 has the best performance with an error rate of 4.37% and an accuracy of 95.63%. The prediction of ovulation time for each female volunteer was carried out in each month of her menstrual cycle through the salivary ferning image dataset using the three methods mentioned above.

2. METHOD

2.1. Pixel counting

Pixel counting is a simple and fast method for predicting a woman's ovulation period by calculating the number of pixels that form a fern-like line structure pattern from salivary images in one woman's menstrual calendar cycle. The most number of pixels in an image of fern-like lines from the results of the

pixel counting method, it is predicted that that day is the peak time for ovulation or release of eggs from the ovaries, which only occurs in one day, as shown in Figure 2. During ovulation, the egg is ready to be fertilized by sperm, resulting in pregnancy. The prediction results from the pixel counting method will be compared with the medical calendar system for women's menstrual cycles; in general, women's ovulation occurs two weeks before the first day of menstruation in the next month's menstrual cycle.

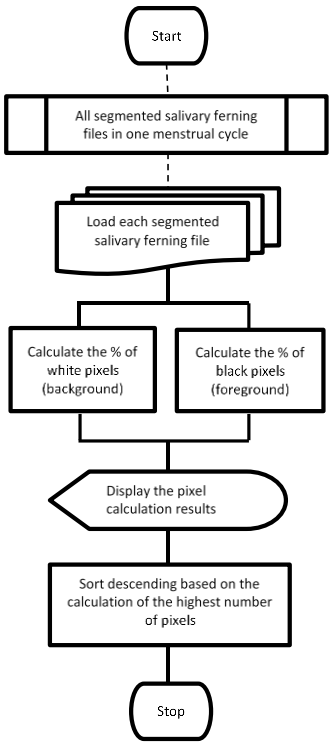

Figure 2. Stages of the pixel counting process

Table 1 is an example of the results of computational processing of salivary ferning images using the pixel counting method to predict the ovulation period of female volunteers whose one menstrual cycle is 25 days in that month. Table 1 can be visualized in a graphic image, as shown in Figure 3, so the ovulation time is predicted to occur on the 12th day. The data is compared with the medical calendar system schedule to see if there is a match. Based on a comparison of the data in Table 1, Figures 3, and 4, it can be concluded that the computational pixel counting results and the medical calendar system for women's menstrual cycles can be compatible.

The results of the prediction of ovulation time from the computational pixel counting process compared to the effects of calculating the time of ovulation using the women's menstrual cycle calendar system in Table 2 have a similarity correspondence of 80%. The data was taken from ten female volunteers with an average menstrual cycle of 23.3 days. This dataset was taken from female volunteers of reproductive age who did not smoke, did not drink alcohol, and did not use contraceptive devices or drugs. The salivary ferning dataset was taken every morning after waking up before eating, drinking, and brushing teeth using the ovutest scope.

In the following section, two other methods are discussed that are used to detect and calculate the presence of pixels that form fern-like lines in salivary ferning; the first method uses box-counting, which is a simple method and has high reliability, often used to measure irregularities and roughness of fractal objects by self-similarity. The right choice is needed to guarantee the accuracy of fractal dimension estimation according to the number of sizes and box size limits. Șerbănescu [12] proposes a box-counting algorithm that can avoid the boundary problem that occurs in changing image sizes by counting squares of fractions instead of integers, thereby enabling the number of squares to be accurate. The second method that will be discussed is the box-counting method which uses deep learning for computer vision to count all the pixels of fern-like lines through several windows or patch sizes.

Table 1. Example of ranking ovulation in a woman's menstrual cycle

Day	Salivary fern image process					Ovulation prediction squence	Pixel counting results	
	Original image	Outlines image	Frangi image	Remove small pixels	Image complement		Black pixels	White pixels
3	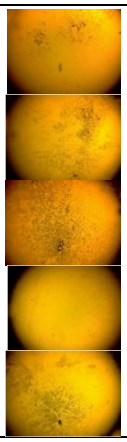					15	16,485	345,618
4						6	45,630	310,479
12						1	84,096	273,204
24						20	6,933	344,409
25						4	48,225	308,781

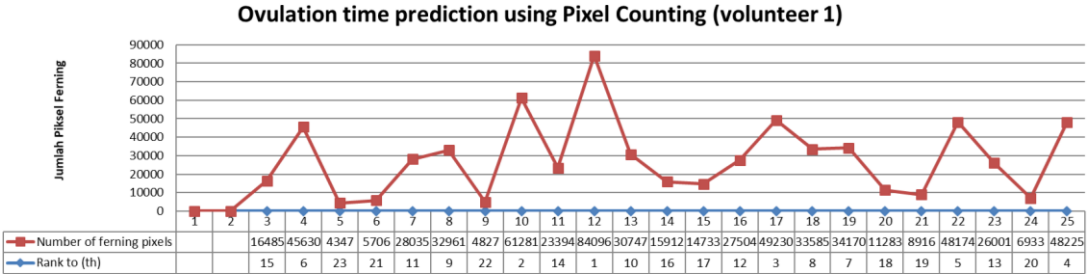

Figure 3. Ovulation chart based on pixel counting

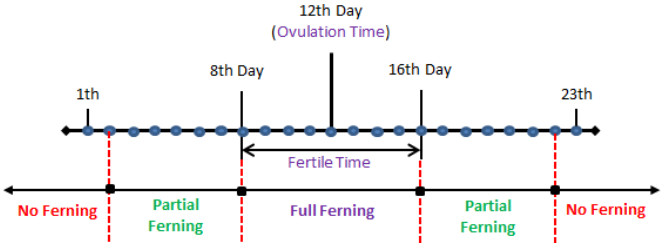

Figure 4. Example chart of a woman's menstrual cycle calendar system

Table 2. Comparison of a calendar system and pixel counting systems

Subject volunteer	Menstrual cycle period (days)	Ovulation day predictions based on pixel counting	Ovulation period based calendar system menstrual cycle	Comparative results	
				Corresponding	Uncoressponding
1st	25	12	08---12---16	Yes	-
2nd	26	07	09---13---17	-	Yes
3rd	24	15	08---12---16	Yes	-
4th	21	20	06---10---14	-	Yes
5th	25	15	08---12---16	Yes	-
6th	22	13	07---11---15	Yes	-
7th	23	08	07---11---15	Yes	-
8th	23	14	07---11---15	Yes	-
9th	18	07	05---09---13	Yes	-
10th	26	18	09---13---17	Yes	-
Average menstrual cycle period		23.3	Similarity	80%	20%

2.2. Box counting

Fractal dimension is an index used in computer vision to characterize fractal patterns by measuring their complexity as the ratio of change in detail to change in scale. A common approach for fractal dimension estimation in binary images is a box-counting algorithm that calculates the number of squares needed to cover objects at different scales. The application of the box-counting method will calculate the fractal dimension values, lacuranity, slope, and the number of boxes that detect the presence of fern-like lines from the salivary ferning image. The fractal dimension (*DF*) is an index of how detail changes with a resolution, based on the notion of dimensionality that arises from $N=R^{-D}$, where N is the number of constituent parts of a pattern counted and R is the relative scale on which the number of elements is measured. In contrast, a complexity measure is calculated in (1), where N is the number of new parts, and ε is the scale. The sloping approach or the slope of the regression line is obtained by (2) with DB as the box-counting fractal dimension.

$$D_F = \log N_\varepsilon / \log \varepsilon \tag{1}$$

$$D_B = \lim_{\varepsilon \to 0} [\log N_\varepsilon / \log \varepsilon] \tag{2}$$

The fractal dimension is calculated from the pixel mass lacunarity (DΛ) with the formula as in (3), where $\lim_{\varepsilon \to 0}$ is obtained as the slope of the regression line, g is the grid orientation, ε is the scale, σ is the standard deviation, and μ is the mean for pixels per square over some ε. While λ is the foreground lacunarity calculated from the relative variation in pixel mass with ε as the over-grid orientation as in (4). The concept of fractals can be applied for image analysis and pattern recognition, and the complexity of geometric shapes or textures of an object can be measured by fractal dimensions [13], [14]. Meanwhile, measuring the spatial distribution of a certain size gap in the image texture can be done by lacunarity [15], [16]. The lacunarity value size indicates that the image's texture is homogeneous or heterogeneous based on the same or unequal gap size. Lacunarity is widely applied to texture-based research fields, including the field of spatial data mapping [17], [18], the agricultural industry [19], and the medical field [20].

$$\Lambda D_g = (\lim_{\varepsilon \to 0} [\, ln\sigma(\varepsilon)/ln\varepsilon]) - ((\lim_{\varepsilon \to 0} [ln\lambda(\varepsilon)/ln\varepsilon])/2) \tag{3}$$

$$\lambda = (\sigma/\mu)^2 \tag{4}$$

Box-counting can be used to calculate fractal dimension values [21] due to the ability and ease of box-counting to represent the complexity of an image [22]. Because the misclassification rate is still relatively high due to the box-counting classification process based on fractal dimension features, combining it with the lacunarity method based on fractal texture features is necessary to improve its accuracy. The fractal dimension cannot distinguish two images with the same repeating pattern, even though the two images have different visual appearances. The weakness of the fractal dimension can be done by lacuranity because it can describe the distribution of gaps in an image and analyze surface heterogeneity in an image.

In this research, the computational process for detecting patterns of fern-like lines in salivary ferning using the box-counting method was carried out in fourteen stages. In each phase, there was a large-scale change from the giant box to the smallest. Figure 5(a) shows the eleventh step of the detection process of the fern-like line pattern from salivary ferning using box counting, Figure 5(b) shows the twelfth of the fourteen stages of the process, and Figure 5(c) shows the stages thirteenth of the box-counting detection process. Meanwhile, Figure 5(d) is the last of the fourteen steps of detecting natural fractal shapes from fern-like lines in salivary ferning.

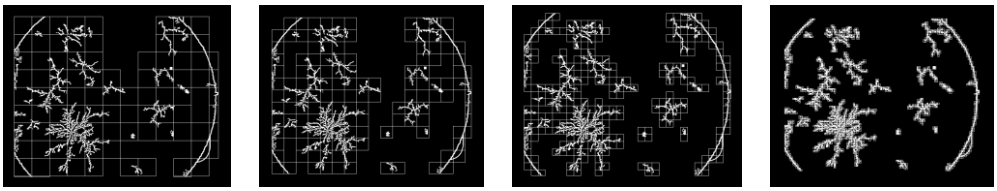

(a) (b) (c) (d)

Figure 5. Computation stages: (a) box-counting stage 11/14, (b) box-counting stage 12/14, (c) box-counting stage 13/14, and (d) box-counting stage 14/14

2.3. Deep learning for computer vision

Deep learning for computer vision [23] as a new technology has great potential in recognizing and detecting surface cracks in objects to improve the structural safety of construction in buildings, highways, and bridges. Some of the previous studies were mainly applied to several things, including detecting cracks in walls and asphalt on streets or being used to detect cracks in steel. In this study, deep learning for computer vision is used to detect the fern-like line of salivary ferning by calculating the number of box counting. The results of detecting fern-like lines and calculating the number of squares counted in each salivary ferning image in one menstrual cycle of a woman can determine her ovulation period. It has been medically proven that at the time of ovulation, the number and shape of the fern-like line pattern in the salivary are highest.

Computer vision functions to understand and interpret images and videos that teach computers how to see and use visual information to perform visual tasks humans can accomplish, especially for predictive studies or decision-making. ResNet is a CNN architecture introduced in 2016 under the title "deep residual learning for image recognition" which won the 2015 ILSVRC challenge [24]. The main innovation of ResNet is the residual identity model, namely: a block of two convolution layers with the same number of filters and a small filter size where the output of the second layer will be added to the input to the first convolution layer, which is called a shortcut connection. This layer is managed with gated units that allow it to pass information to the next convolution layer; ResNet uses batch normalization to improve the stability of its network, as shown in Figure 6.

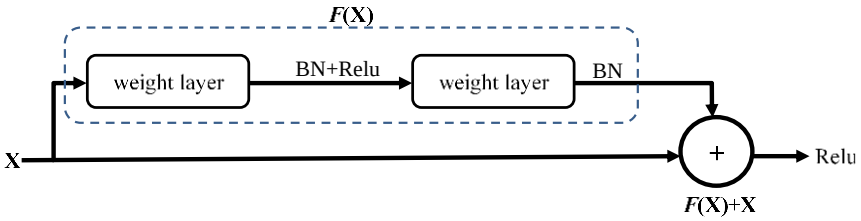

Figure 6. Residual module ResNet

Deep learning uses ResNet to solve image classification and computer vision problems through deep CNN training methods with stochastic depth [25]. Investigation of medical image classification of the colon glands using deep learning methods with ResNet-18 and ResNet-50 architectures to detect malignant or benign colorectal cancer [26]. Detection of wood knot defects using a combination of ResNet-18 and transfer learning with an accuracy of up to 99.02% [27], while retrieval of multimodal medical image datasets using ResNet-18 which contains twenty-three classes and four modalities, including computed tomography (CT), magnetic resonance imaging (MRI), mammogram (MG), and positron emission tomograph (PET) with an average classification accuracy of 92% [28].

In recent years, studies using ResNet-34 include: the combination of ResNet-34 and transfer learning as a feature extractor for wood knot defects can significantly increase the final prediction accuracy of wood knot defect detection [29]. Meanwhile, developing a computationally efficient and scalable deep learning model using a CNN based on the ResNet-34 architecture to diagnose DR automatically with classification results through F1-score measurements of 93.2% [30]. Research to identify 18 typologically different languages from speech recordings, cel-frequency cepstral coefficients originating from audio files were converted into spectrograms, which were then incorporated into the CNN architecture based on ResNet-50 with the final result being validation accuracy of 73% and testing accuracy of 53% [31]. Meanwhile, the application of ResNet-50 with a convolution layer depth of 25 to diagnose three anomaly image datasets, namely; bottles, spoons, and cartons, the prediction accuracy of the three datasets is 99%, 95%, and 90% [32]. In this study, we will compare the results of detecting fern-like lines using deep learning with ResNet-18, ResNet-34, and ResNet-50 architectures.

3. RESULTS AND DISCUSSION

This study is the first to predict female ovulation time through fern-like lines from salivary ferning at its peak (full ferning). The first method is calculating the fractal dimensions of fern-like lines using box counting. The second is to calculate the box-counting number of fern-like lines using computer vision using deep learning with pre-trained CNN model ResNet-18 architecture, ResNet-34, and ResNet-50. An explanation of the empirical results will be discussed in the following section.

3.1. Box-counting

Based on the binary image in Figure 1(b), a computational process is carried out using the box-counting method to measure the fractal dimension. The final result of the computational process using the box-counting method looks like in Figure 5(d). The parameter values of the fractal dimension, lacuranity, slope, foreground pixels, and total pixels in Figure 5(d) can be seen in Table 3, and the shape of the slope graph is shown in Figure 7. The fractal dimensions form the fern-like pattern in Figure 5(d) is 1.4738, which is a fractional dimension, unlike Euclidean's geometry, which is an integer dimension, so it cannot calculate the fractal dimension in Figure 1(b). Besides that, the fractal dimension can describe irregularities and how much space an object occupies.

Table 3. The fractal dimension parameter value of fern-like lines image

Fractal dimension	Lacuranity	Slope	Foreground pixels (white colour)	Total pixels
1.4738	0.6442	0.0244	20,499	293,627

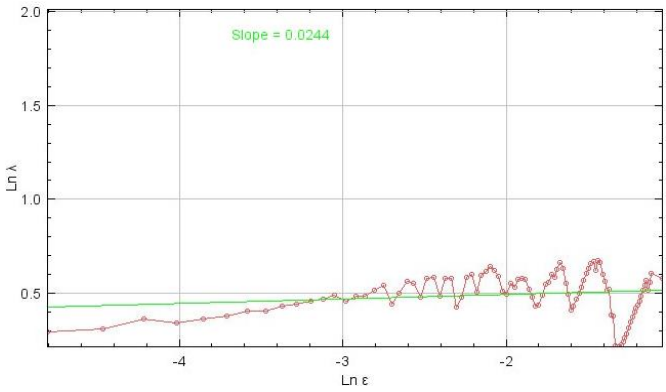

Figure 7. Slope graph display from fern-like lines image

The lacunarity value of the fern-like line pattern in Figure 1(b) is 0.6442; a low lacunarity value means the texture is homogeneous; conversely, the higher the lacuranity value, the object texture is heterogeneous, which means that the pixels spread over a wide range and are surrounded by large gaps. The slope value of Figure 5(d) in this study is 0.0244, with a graphical appearance that looks like in Figure 7, the slope is the slope of a straight line, and the value of this slope is the fractal dimension of an image. The least squares method can calculate a straight line's slope or slope value. Meanwhile, the number of white pixels that form the fern-like lines in Figure 5(d) as the foreground is 20,499 pixels.

3.2. Deep learning

The total number of salivary ferning image datasets in this study is 3,779,000 pieces with a resolution size of 227x227 pixels; 50% of the dataset is used for the training process, 30% for validation, and 20% for the testing process. The dataset was taken from 10 female volunteers aged between 20-40 years for three consecutive months with an average menstrual cycle of 24 days. In this study, to detect the time of female ovulation through deep learning for computer vision, a comparison was made of three pre-trained network model CNN architecture models: ResNet-18, ResNet-34, and ResNet-50. The fern-like lines pattern in salivary ferning has a natural fractal shape to detect in this study using the box-counting method with windows or patch sizes of 32x32 pixels, 16x16 pixels, and 8x8 pixels on the three ResNet pre-trained network models mentioned above.

Based on Table 4, the training process was carried out for 5 epochs with a learning rate of 1e-3 which obtained the optimal valley point at 0.0014454398 with the highest accuracy results on patch sizes of 32x32 pixels and 16x16 pixels obtained by ResNet-50 of 95.36%, while for patch sizes 8x8 pixel patch with the highest accuracy of 94.97% obtained by ResNet-34. The results of the validation process are shown in Figure 8 by using the auto-learning rate (1e-3–1e-4) so that the optimal valley point can be searched automatically by the system, with the highest accuracy with a 32x32 pixel patch size of 98.16% and 16x16 pixels with 98.54% obtained by ResNet-50, while at a patch size of 8x8 pixels pretrained network ResNet-34 has the highest accuracy of 98.28%. The accuracy of the auto-learning rate (1e-3–1e-4) is higher than the accuracy of the manual learning rate (1e-3).

The confusion matrix values, as shown in Table 5, can be used to calculate the parameter values of precision, recall, F1-score, and accuracy of all misclassification images through independent test sets.

ResNet-50 with a patch size of 32x32 pixels has the highest accuracy of 99.88%; for a patch size of 16x16 pixels, the highest accuracy is obtained by ResNet-18 of 100%, while for patch sizes of 8x8 pretrained network models, ResNet-34 and ResNet-50 have high accuracy the same amounting to 99.77%.

Table 4. Accuracy results from the training process using learning rate 1e-3

Windows size (patches)	Pre-trained network	Find the best learning The rate for training (lr_max=1e-3)						Results on the validation set confusion matrix			
		Epoch	Train_loss	Valid_loss	Error_rate	Accuracy	Time	TP	TN	FP	FN
32x32 pixel	ResNet18	5th	0.488587	0.208071	0.047682	0.952318	00:15	60	660	24	12
	ResNet34		0.483574	0.214148	0.059603	0.940397	00:16	63	649	29	14
	ResNet50		0.357584	0.222505	0.046358	0.953642	00:27	60	660	18	17
16x16 pixel	ResNet18		0.492976	0.242286	0.060927	0.939073	00:15	61	648	30	16
	ResNet34		0.472387	0.229613	0.059603	0.940397	00:17	61	649	29	16
	ResNet50		0.362134	0.240714	0.046358	0.953642	00:27	62	658	20	15
8x8 pixel	ResNet18		0.480596	0.210464	0.055629	0.944371	00:15	59	654	24	18
	ResNet34		0.482746	0.204411	0.050331	0.949669	00:17	56	661	17	21
	ResNet50		0.359593	0.326643	0.056954	0.943046	00:27	66	646	32	11

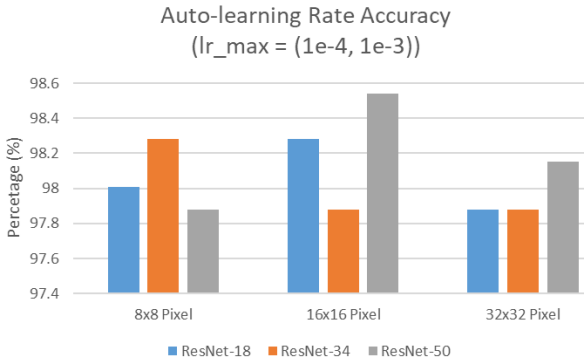

Figure 8. Accuracy graph display from auto-learning rate

Table 5. The results of the measurement of the independent test set

Windows size (patches)	Pre-trained network	Check all the misclassifications (10 images)		Independent test set				Results on the validation set confusion matrix			
		Loss average	Probability average	Precision	Recall	F1-score	Accuracy	TP	TN	FP	FN
32x32 pixel	ResNet18	9.185	0.921	0.98	1.00	0.99	0.99648	132	717	3	0
	ResNet34	2.85	0.83	0.98	0.97	0.97	0.99648	132	717	3	0
	ResNet50	9.849	0.815	0.99	1.00	1.00	0.99883	132	719	1	0
16x16 pixel	ResNet18	6.405	0.845	1.00	1.00	1.00	1.0	132	720	0	0
	ResNet34	9.194	0.919	0.98	1.00	0.99	0.99648	132	717	3	0
	ResNet50	21.179	0.917	0.99	1.00	0.99	0.99765	132	718	2	0
8x8 pixel	ResNet18	14.474	0.96	0.96	1.00	0.98	0.99413	132	715	5	0
	ResNet34	16.221	0.792	0.99	0.99	0.99	0.99765	131	719	1	1
	ResNet50	6.969	0.88	0.99	1.00	0.99	0.99765	132	718	2	0

The visual display of the detection results from the fractal fern-like lines pattern of the salivary ferning image with windows size (32x32 pixels) is shown Figure 9. The pre-trained network model ResNet-18 used in Figure 9(a) has the highest number of patches, namely 114 patches (116,736 pixels), in comparison, the ResNet-34 model used in Figure 9(b) has 91 patches (93,184 pixels), and the ResNet-50 model used in Figure 9(c) has 107 patches (109,568 pixels). Figure 10 displays the results of detecting fern-like lines fractal patterns from salivary ferning images with windows size (16x16 pixels), the pre-trained network model ResNet-18 used in Figure 10(a) has a total of 153 patches (39,168 pixels), in contrast, the ResNet-34 model used in Figure 10(b) has the largest number of patches, namely 287 patches (73,472 pixels), and the ResNet-50 model used in Figure 10(c) has 175 patches (44,800 pixels). Figure 11 shows visualization of the shape of the fractal fern-like lines pattern from the salivary ferning image with a windows size (8x8 pixels); the pre-trained network model ResNet-18 used in Figure 11(a) has a total of 527 patches (33,728 pixels), while the ResNet-34 model used in Figure 11(b) has the largest number of patches, namely 568 patches (36,352 pixels) and the ResNet-50 model shown used in Figure 11(c) only has 1 patch (64 pixels).

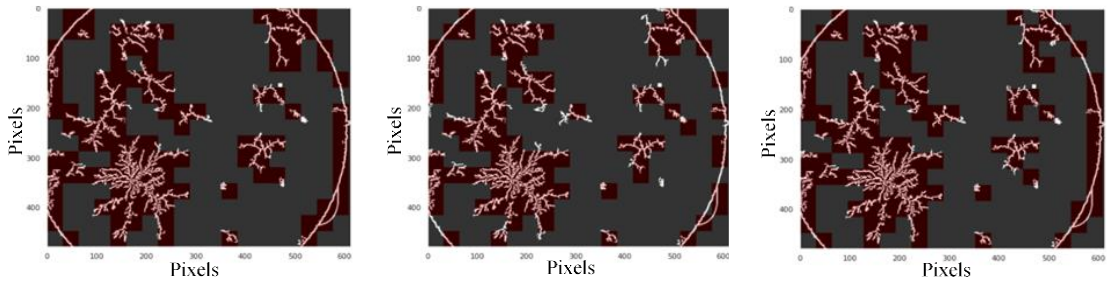

Figure 9. Visualization of fern-like strain detection results using a window size of 32x32 pixels: (a) ResNet-18, (b) ResNet-34, and (c) ResNet-50

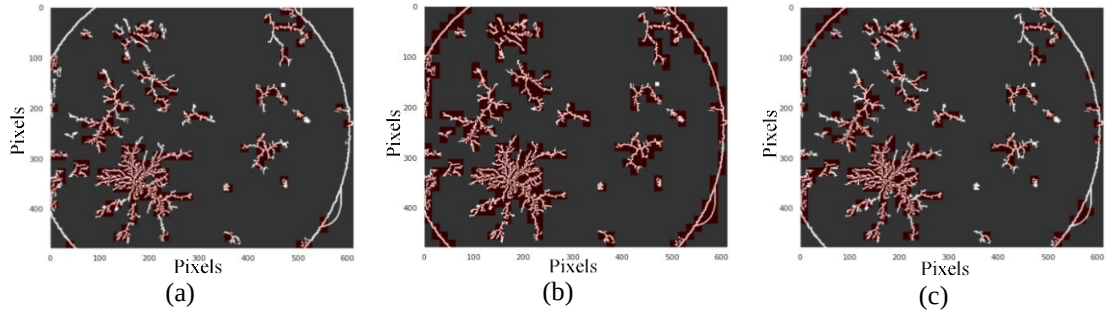

Figure 10. Visualization of fern-like strain detection results using a window size of 16x16 pixels: (a) ResNet-18, (b) ResNet-34, and (c) ResNet-50

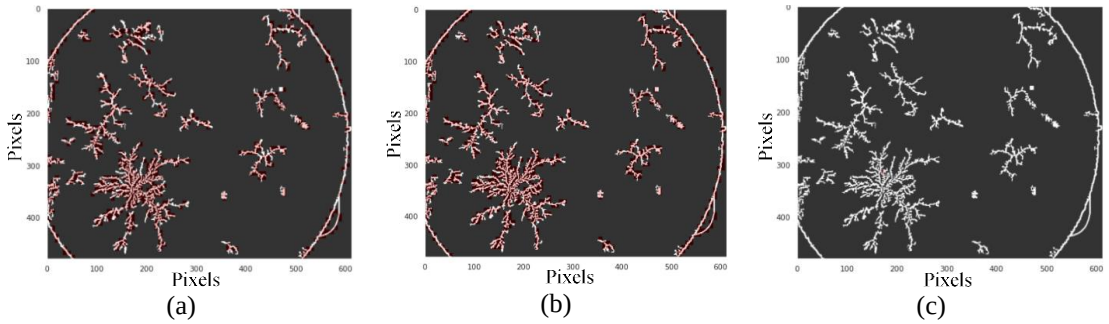

Figure 11. Visualization of fern-like strain detection results using a window size of 8x8 pixels: (a) ResNet-18, (b) ResNet-34, and (c) ResNet-50

4. CONCLUSION

The main novelty of this study is how to predict the time of ovulation in women through visualization of the detection of natural fractal dimensions from the fern-like lines pattern in salivary ferning using three different methods, namely: pixel counting, box counting, and patch counting with three different window sizes (8x8, 18x18, and 32x32 pixels) using deep learning. It has been medically proven that when ovulation occurs, the number of fern-like lines in a woman's saliva reaches its peak; this condition is known as FF. The computational pixel counting method is performed on all salivary ferning images from ten female volunteers each month in one menstrual cycle. The results of pixel counting calculations with the most pixels that form fern-like lines in each menstrual cycle are predicted as FF conditions, which means that ovulation occurs. These results will be compared with the medical menstrual cycle calendar system, which states that ovulation occurs two weeks before the first day of menstruation in the following month with an accuracy of 80%.

The box-counting method, supported by the sliding box method from lacuranity, can also detect FF conditions by calculating the shape of the natural fractal dimension 1.4738 from the image of fern-like lines in salivary ferning. Besides that, you can also do calculations at the pixel level with a total of

20,499 pixels that make up the fern-like lines pattern. In the training process in applying the deep learning for computer vision method using the pre-trained network ResNet model, there was an average increase in accuracy of 3,459% from using the manual learning rate (1e-3) to the auto-learning rate (1e-4, 1e-3). At the stage of the training process with a total of 5 epochs and 1e-3 learning, the ResNet-50 pretrained network model has the highest accuracy of 95.36% on windows sizes of 32x32 pixels and 16x16 pixels.

For the validation process stage using the auto-learning rate (1e-3, 1e-4), the highest accuracy of 98.54% was achieved by ResNet-50 on a 16x16 pixel window size scale. In comparison, in the classification stage, the pre-trained network model ResNet-18 attained an accuracy of up to 100 % in windows size 32x32 pixels with a precision of 1.00, recall 1.00, and F1-score 1.00. During the results of the visualization of the process of detecting fern-like lines in deep learning for computer vision on windows size 8x8 pixels, the ResNet-34 model gets the most number of patches, namely: 568 patches (36,352 pixels). Furthermore, this research can develop the process of detecting fern-like line patterns from salivary ferning through heatmaps and saliency maps using the gradient class activation map or attention layer method.

REFERENCES

[1] H. Pratikno and M. Z. Ibrahim, "Image Segmentation of Women's Salivary Ferning Patterns Using Harmony Frangi Filter," *Lecture Notes in Electrical Engineering*, vol. 632, pp. 605–622, 2020, doi: 10.1007/978-981-15-2317-5_51.

[2] H. M. Eissa, A. M. Ahmed, and E. A. Elsehely, "Implementation of smart ovulation detection device," *Recent Adv Biomed Chem Eng Mater Sci*, no. March 2014, pp. 82–86, 2014.

[3] H. C. Wu, C. Y. Lin, S. H. Huang, and M. H. Tseng, "An intelligent saliva recognition system for women's ovulation detection," *Lecture Notes in Computer Science (including subseries Lecture Notes in Artificial Intelligence and Lecture Notes in Bioinformatics)*, vol. 9011, pp. 614–623, 2015, doi: 10.1007/978-3-319-15702-3_59.

[4] R. Ravinder *et al.*, "Saliva ferning, an unorthodox estrus detection method in water buffaloes (Bubalus bubalis)," *Theriogenology*, vol. 86, no. 5, pp. 1147–1155, 2016, doi: 10.1016/j.theriogenology.2016.04.004.

[5] A. Kubátová and T. Fedorova, "Saliva crystallization occurs in female bornean orangutans (Pongo pygmaeus): Could it be a new option for monitoring of menstrual cycle in captive great apes?," *PLoS ONE*, vol. 11, no. 7, p. e0159960, Jul. 2016, doi: 10.1371/journal.pone.0159960.

[6] V. Potluri *et al.*, "An inexpensive smartphone-based device for point-of-care ovulation testing," *Lab on a Chip*, vol. 19, no. 1, pp. 59–67, 2019, doi: 10.1039/c8lc00792f.

[7] L. Luo, X. She, J. Cao, Y. Zhang, Y. Li, and P. X. K. Song, "Detection and Prediction of Ovulation from Body Temperature Measured by an In-Ear Wearable Thermometer," *IEEE Transactions on Biomedical Engineering*, vol. 67, no. 2, pp. 512–522, Feb. 2020, doi: 10.1109/TBME.2019.2916823.

[8] D. Ristanović, B. D. Stefanović, and N. Puškaš, "Fractal analysis of dendrite morphology using modified box-counting method," *Neuroscience Research*, vol. 84, pp. 64–67, 2014, doi: 10.1016/j.neures.2014.04.005.

[9] N. Maryenko and O. Stepanenko, "Characterization of white matter branching in human cerebella: quantitative morphological assessment and fractal analysis of skeletonized MR images," *Biomedical Research and Therapy*, vol. 8, no. 5, pp. 4345–4357, 2021, doi: 10.15419/bmrat.v8i5.673.

[10] S. S. Devi and S. Vidivelli, "Modified differential box counting in breast masses for bioinformatics applications," *Computers, Materials and Continua*, vol. 70, no. 2, pp. 3049–3066, 2022, doi: 10.32604/cmc.2022.019917.

[11] H. Pratikno, M. Z. Ibrahim, and Jusak, "A novel fern-like lines detection using a hybrid of pre-trained convolutional neural network model and Frangi filter," *TELKOMNIKA (Telecommunication Computing Electronics and Control)*, vol. 20, no. 3, pp. 607–620, Jun. 2022, doi: 10.12928/TELKOMNIKA.v20i3.23319.

[12] M. S. Șerbănescu, "Fractal Dimension Box-Counting Algorithm Optimization Through Integral Images," *IFMBE Proceedings*, vol. 88, pp. 95–101, 2022, doi: 10.1007/978-3-030-93564-1_11.

[13] C. Allain and M. Cloitre, "Characterizing the lacunarity of random and deterministic fractal sets," *Physical Review A*, vol. 44, no. 6, pp. 3552–3558, Sep. 1991, doi: 10.1103/PhysRevA.44.3552.

[14] P. Dong and P. Dong, "Test of a new lacunarity estimation method for image texture analysis," *International Journal of Remote Sensing*, vol. 21, no. 17, pp. 3369–3373, 2000, doi: 10.1080/014311600750019985.

[15] B. Burlando, "The fractal geometry of evolution," *Journal of Theoretical Biology*, vol. 163, no. 2, pp. 161–172, 1993, doi: 10.1006/jtbi.1993.1114.

[16] A. R. Backes, "A new approach to estimate lacunarity of texture images," *Pattern Recognition Letters*, vol. 34, no. 13, pp. 1455–1461, Oct. 2013, doi: 10.1016/j.patrec.2013.05.008.

[17] S. W. Myint and N. Lam, "A study of lacunarity-based texture analysis approaches to improve urban image classification," *Computers, Environment and Urban Systems*, vol. 29, no. 5 SPEC. ISS., pp. 501–523, Sep. 2005, doi: 10.1016/j.compenvurbsys.2005.01.007.

[18] P. Dong, "Lacunarity analysis of raster datasets and 1D, 2D, and 3D point patterns," *Computers and Geosciences*, vol. 35, no. 10, pp. 2100–2110, Oct. 2009, doi: 10.1016/j.cageo.2009.04.001.

[19] L. Li, L. Chang, S. Ke, and D. Huang, "Multifractal analysis and lacunarity analysis: A promising method for the automated assessment of muskmelon (Cucumis melo L.) epidermis netting," *Computers and Electronics in Agriculture*, vol. 88, pp. 72–84, Oct. 2012, doi: 10.1016/j.compag.2012.06.006.

[20] P. Borys, M. Krasowska, Z. J. Grzywna, M. B. A. Djamgoz, and M. E. Mycielska, "Lacunarity as a novel measure of cancer cells behavior," *BioSystems*, vol. 94, no. 3, pp. 276–281, Dec. 2008, doi: 10.1016/j.biosystems.2008.05.036.

[21] R. F. Voss, "Characterization and measurement of random fractals," *Physica Scripta*, vol. 1986, no. T13, pp. 27–32, Jan. 1986, doi: 10.1088/0031-8949/1986/T13/004.

[22] K. I. Kilic and R. H. Abiyev, "Exploiting the synergy between fractal dimension and lacunarity for improved texture recognition," *Signal Processing*, vol. 91, no. 10, pp. 2332–2344, Oct. 2011, doi: 10.1016/j.sigpro.2011.04.018.

[23] C. Yang, J. Chen, Z. Li, and Y. Huang, "Structural crack detection and recognition based on deep learning," *Applied Sciences (Switzerland)*, vol. 11, no. 6, p. 2868, Mar. 2021, doi: 10.3390/app11062868.

[24] K. He, X. Zhang, S. Ren, and J. Sun, "Deep residual learning for image recognition," in *Proceedings of the IEEE Computer Society Conference on Computer Vision and Pattern Recognition*, IEEE, Jun. 2016, pp. 770–778, doi: 10.1109/CVPR.2016.90.

[25] K. E. Tokarev, V. M. Zotov, V. N. Khavronina, and O. V. Rodionova, "Convolutional neural network of deep learning in

computer vision and image classification problems," *IOP Conference Series: Earth and Environmental Science*, vol. 786, no. 1, p. 012040, Jun. 2021, doi: 10.1088/1755-1315/786/1/012040.
[26] D. Sarwinda, R. H. Paradisa, A. Bustamam, and P. Anggia, "Deep Learning in Image Classification using Residual Network (ResNet) Variants for Detection of Colorectal Cancer," *Procedia Computer Science*, vol. 179, pp. 423–431, 2021, doi: 10.1016/j.procs.2021.01.025.
[27] M. Gao, P. Song, F. Wang, J. Liu, A. Mandelis, and D. Qi, "A Novel Deep Convolutional Neural Network Based on ResNet-18 and Transfer Learning for Detection of Wood Knot Defects," *Journal of Sensors*, vol. 2021, pp. 4428964:1-4428964:16, 2021, doi: 10.1155/2021/4428964.
[28] V. Alex, M. Khened, S. Ayyachamy, and G. Krishnamurthi, "Medical image retrieval using Resnet-18 for clinical diagnosis," in *Medical Imaging 2019: Imaging Informatics for Healthcare, Research, and Applications*, P. R. Bak and P.-H. Chen, Eds., SPIE, Mar. 2019, p. 35, doi: 10.1117/12.2515588.
[29] M. Gao, J. Chen, H. Mu, and D. Qi, "A transfer residual neural network based on resnet-34 for detection of wood knot defects," *Forests*, vol. 12, no. 2, pp. 1–16, Feb. 2021, doi: 10.3390/f12020212.
[30] N. M. Al-Moosawi and R. S. Khudeyer, "ResNet-34/DR: A Residual Convolutional Neural Network for the Diagnosis of Diabetic Retinopathy," *Informatica (Slovenia)*, vol. 45, no. 7, pp. 115–124, 2021, doi: 10.31449/inf.v45i7.3774.
[31] G. G. A. Celano, "A ResNet-50-based Convolutional Neural Network Model for Language ID Identification from Speech Recordings," in *SIGTYP 2021 - 3rd Workshop on Research in Computational Typology and Multilingual NLP, Proceedings of the Workshop*, Stroudsburg, PA, USA: Association for Computational Linguistics, 2021, pp. 136–144, doi: 10.18653/v1/2021.sigtyp-1.13.
[32] Z. T. Omer and A. H. Abbas, "Image anomalies detection using transfer learning of resnet-50 convolutional neural network," *Indonesian Journal of Electrical Engineering and Computer Science*, vol. 27, no. 1, pp. 198–205, Jul. 2022, doi: 10.11591/ijeecs.v27.i1.pp198-205.

BIOGRAPHIES OF AUTHORS

Heri Pratikno obtained Magister Teknik (M.T) in the Electrical Engineering Study Program-Intelligent Multimedia Network from the Institut Teknologi Sepuluh Nopember (ITS), Indonesia. He is currently working at University Dinamika, Indonesia, and is a Ph.D candidate at the Faculty of Electrical and Electronic Engineering Technology of University Malaysia Pahang, Malaysia. His research interests are computer vision, image processing, deep learning, IoT, computer networking, and network security. He can be contacted at email: heri@dinamika.ac.id.

Mohd Zamri Ibrahim obtained both B.Eng and M.Eng in Electrical Engineering from University Teknologi Malaysia, Malaysia, and a Ph.D in Electrical and Electronics Engineering from Loughborough University, United Kingdom. His research interests are computer vision, the internet of things, embedded system programming, brain-computer interaction, image processing, intelligent system, and speech recognition. He is a senior lecturer at the Faculty of Electrical and Electronic Engineering Technology of University Malaysia Pahang Al-Sultan Abdullah, Malaysia. He has received more than 10 awards at national and international research exhibitions and is currently a principal investigator on TERAJU RM500K project on the Portable Vein Finder imaging device. Before joining University Malaysia Pahang Al-Sultan Abdullah, He was a procurement engineer at Hewlett-Packard (HP) Malaysia, where he worked as the primary technical interface with suppliers and HP design center (Vancouver and San Diego) to drive cost reduction, quality improvement, and assurance of supply. He can be contacted at email: zamri@umpsa.edu.my.

Jusak Jusak received B.S degree in Electrical Engineering from Brawijaya University, Malang, Indonesia, in 1996 and a Ph.D degree In Electrical Engineering from Royal Melbourne Institute of Technology (RMIT) University, Melbourne, Australia, in 2006. From 2009 to 2011, he was a Postdoctoral Research with Massey University, Palmerston North, New Zealand, working in a Next Generation Networks research project supported the Telecom New Zealand. Between 2011 and 2021, he was a Senior Lecturer in Department of Computer Engineering at Dinamika University, Surabaya, Indonesia. He is currently a Senior Lecturer in IoT at James Cook University Singapore. His research interest includes signal processing for wireless communication networks, biomedical signal processing, and the Internet of Things for medical applications and their security. He was a recipient of a Ph.D research award in 2004. He received several national-level research competitive grants from 2011 to 2020 and the best paper award at the International Conference on Information Technology Applications and Systems in 2018. He can be contacted at email: jusak@dinamika.ac.id.